# esteem3

Enabling Science through European Electron Microscopy

Report on comparison of precision versus dose for imaging and diffraction methods

Deliverable D4.3 – version 1.2

Estimated delivery date:	30.04.2023
Actual delivery date:	05.05.2023
Lead beneficiary:	UOFX
Person responsible:	Peter Nellist
Deliverable type:	☒ R ☐ DEM ☐ DEC ☐ OTHER ☐ ETHICS ☐ ORDP
Dissemination level:	☒ PU ☐ CO ☐ EU-RES ☐ EU-CON ☐ EU-SEC
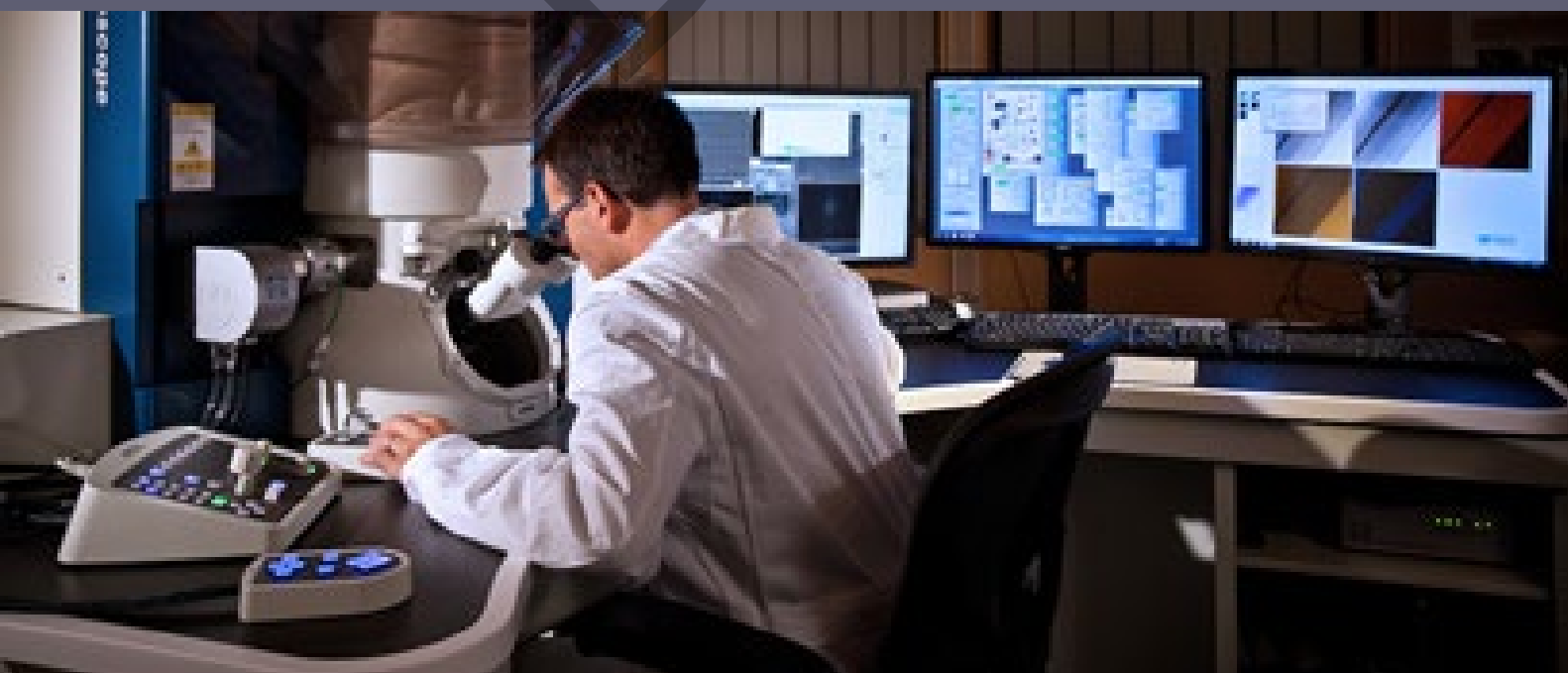
Grant Agreement No:	823717
Funding Instrument:	Research and Innovation Actions (RIA)
Funded under:	H2020-INFRAIA-2018-1: Integrating Activities for Advanced Communities
Starting date:	01.01.2019
Duration:	54 months

Table of contents

Revision history log

Version number	Date of release	Author	Summary of changes
V0.1	18 April 2022	Peter Nellist	First draft of the deliverable
V1.0	03.05.2023	Peter van Aken	Minor amendments and approval
V1.1	04.05.2023	Aude Garsès	Minor amendments and final review

Draft

Executive Summary

The impact of dose on the precision of atomic positions in images is evaluated and on an atom counting method using a combination of imaging and spectroscopic mapping. Finally, the importance of diffraction for phase identification in a highly beam sensitive material is highlighted.

Context and landscape of work

One of the current major challenges in high-resolution characterisation of materials using electron microscopy is its application to materials that are susceptible to damage under the electron beam. This is a problem well-known for biological materials, but is of increasing importance also in physical sciences. Challenges associated with energy storage (for example battery materials) energy conversion (for example nanoparticle and zeolite catalysts), polymer recycling and degradation, as a few examples, all involve beam sensitive materials.

Our ability to use low-dose methods in high-resolution electron microscopy has been revolutionised in particular by the development of direct-electron detectors that have a sufficiently high detector quantum efficiency (DQE) that the noise in any image or diffraction pattern is controlled by the finite electron counting statistics. These detectors have allowed for the establishment of methods in cryo-electron microscopy such as single particle analysis for biological samples. The purpose of this report is to highlight work done within the ESTEEM3 programme to evaluate the impact of low-doses on the quantitative interpretation and metrology from a range of established and emerging techniques that form part of the ESTEEM3 Joint Research Activities. Research themes highlighted are strain mapping from atomic-resolution imaging, quantitative atom counting with elemental specificity and the application of low-dose scanning electron diffraction to hybrid perovskite materials.

Precision of strain measurement under low-doses

The ability to image individual atoms and atomic columns in (scanning) transmission electron microscopy creates the opportunity to directly map lattice distortions in the form of strain. Methods were developed under the ESTEEM2 programme to correct for imaging and scan distortions in the image (Jones *et al.*, 2018). Building on that work, and as part of the metrology work package (WP4) within ESTEEM3, methods have been developed to measure lattice displacements, convert those to a strain tensor that can then be expressed in any coordinate system including in terms of principal strains (Luo *et al.*, 2022). As part of that work, the precision of the strain measurement was evaluated as a function of dose.

Peak finding in annual dark-field (ADF) scanning transmission electron microscope (STEM) images was used to identify displacements due to elastic strain. This can be done by comparing the positions of fitted peaks in the image with a reference lattice. The accuracy of this process will be influenced by the Poisson noise arises from low doses and by the intensity of the peak which is dependent on the number of atoms in an atomic column. The influence of both these parameters is shown in Figure 1 below.
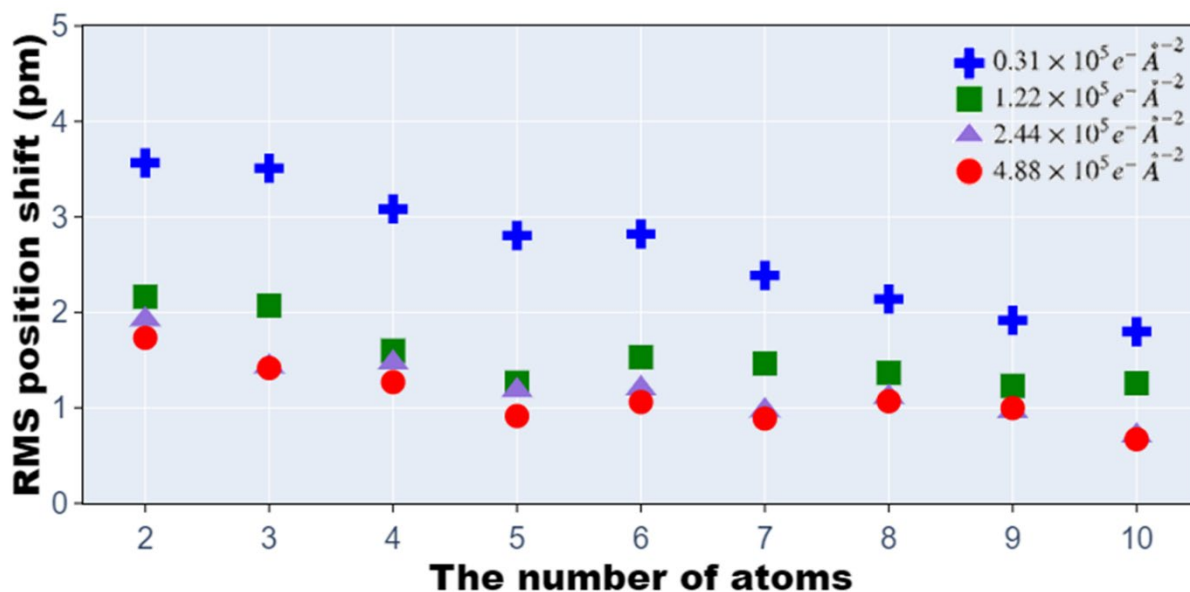
Figure 1. The detected root mean square position shift as a function of number of atoms in an atomic column in the simulated Poisson-distributed images of the perfect Pt model under the different electron doses. From Reference (Luo *et al.*, 2022).

In order to better understand the effect of the noise, Poisson noise under typically single-frame $(0.31 \times 10^5 e^- \text{Å}^{-2})$, low $(1.22 \times 10^5 e^- \text{Å}^{-2})$, medium $(2.44 \times 10^5 e^- \text{Å}^{-2})$ and high $(4.88 \times 10^5 e^- \text{Å}^{-2})$ electron doses, was added to simulated ADF images of perfect (zero-strain) and strained Pt models, respectively. The Poisson noise is added by replacing each pixel with a value selected randomly from a Poisson distribution with a mean given by the simulated number of electron counts. The determined atomic column positions in the simulated images of the perfect Pt model were compared with the real atom positions of the model averaged along a column, the distances between them are defined as the position shifts. Figure 1 shows the measured RMS position shift as a function of number of atoms in an atomic column under the multiple noise realisations. For those atomic columns having more than 4 atoms, the accuracy of the atomic column position finding reaches 1 pm under the medium or high electron dose. The accuracy could be improved as the scattered intensity of the atomic column increases (higher electron dose or more atoms).

Atom counting with elemental specificity

Most imaging modes in the STEM, such as ADF imaging and EDX mapping, are incoherent leading to a monoatomic dependence on the number of atoms present and facilitating paths to quantification and metrology. Methods for atom counting in single element materials, such as catalyst nanoparticles, were established during the ESTEEM2 programme (see for example (Aarons *et al.*, 2017)). In ESTEEM3, these methods have been expanded to the quantification of different element types in mixed element systems (De Backer *et al.*, 2022).

The main challenge is to estimate the two scaling parameters for the EDX cross-sections of the two types of elements. The method developed here makes use of large number of statistics (a large number of atomic columns in multiple images and spectroscopic maps). It is assumed that the experimental HAADF scattering cross-section requires no scaling with respect to simulation as established in the previous work.

5

For a single atomic column, because of the unknown EDX scaling parameters, there is an ambiguity between sample thickness and composition. It is, however, possible to determine an upper and lower bound to the thickness from the HAADF scattering cross-section by assuming the column is either entirely the lighter or heavier species respectively. For each possible thickness, only one column composition can then match the HAADF scattering cross-section, allowing the EDX scaling parameters then to be determined for that composition. By repeating this for all possible thicknesses compatible with the HAADF scattering cross-section, it becomes clear that a finite range of possible EDX scaling parameters for that single column is possible. For a sample with variations in thickness and composition, different columns will lead to different possible ranges of scaling parameters. With sufficient atomic columns in an experiment, the scaling parameters that are most compatible with all of the columns can be determined.

As a proof-of-principle demonstration, Figure 2 shows the absolute quantification of the number of Au and Ag atoms in a core-shell nanorod system.
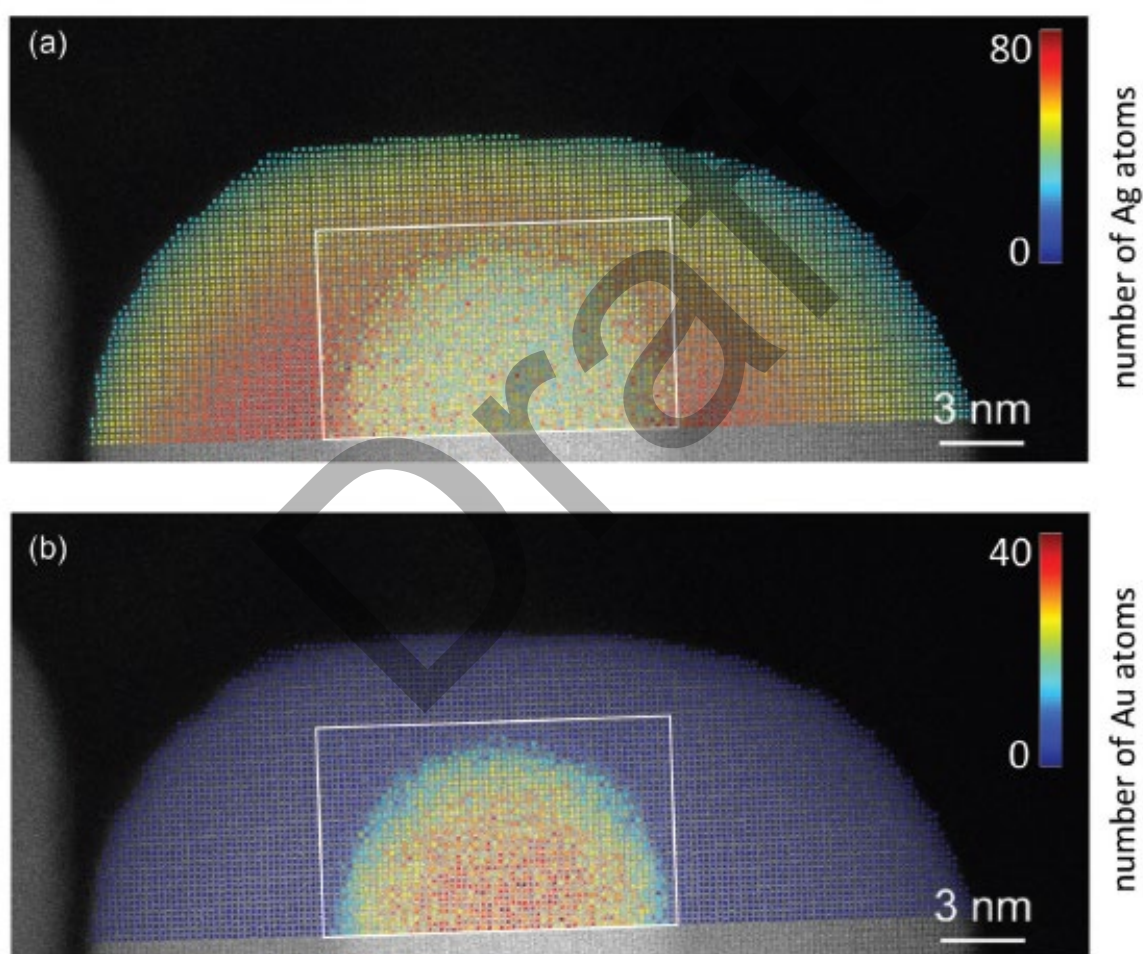

Figure 2. Number of a) Ag and b) Au atoms, shown as an overlay on the experimental HAADF STEM images of an Au@Ag core–shell nanorod. The white square indicates the region where Ag and Au atoms are counted by combining EDX and HAADF STEM imaging.

For the HAADF STEM image an incident electron dose of $3.6 10^4$ e$^-$Å^{-2} per frame was used and for the EDX elemental maps 4.3×10^6 e$^-$Å^{-2}. The question now arises of the precision of this multi-element atom counting process as such doses. Table 1 below shows the root-mean-squared error (RMSE) of the atom counting process.

Type	Total number of atoms ± error	Average error in a column
Ag	(114 037 ± 691) atoms	± 5.6 atoms
Au	(37 083 ± 339) atoms	± 2.5 atoms
Total number of atoms (Ag + Au)	(151 120 ± 370) atoms	± 3.2 atoms

Table 1. Summary of the RMSE on the total number of atoms and the average error on the estimated number of atoms in a column for Ag, Au, and the total number of atoms for the Au@Ag core–shell nanorod. From Reference (De Backer *et al.*, 2022).

The RMSE is a bit larger for the lighter Ag atoms as compared to the RMSE for the Au atoms or the total number of atoms. The error is larger for the mixed columns containing atoms from both the Au core and the Ag shell.

Scanning electron diffraction at low doses

The previous two methods are based on imaging approaches. Electron diffraction can be highly effective for very beam sensitive materials, because the nature of a diffracted beam is that it is expressing positional correlations over a very high number of atoms. Real-space information can still be made available through the use of scanning electron diffraction (SED), but at a lower spatial resolution than imaging.

As an example of this approach, SED has been applied to the study of phase changes in the degradation of a hybrid perovskite material for photovoltaic applications (Figure 3) (Macpherson *et al.*, 2022). These materials are extremely beam sensitive through the dissociation and loss of the organic species in the lattice. To enable phase identification in this material, a dose of 6 e$Å^{-2}$ was used, which kept it well below the established critical dose for this material which is around 66 e$Å^{-2}$. These are much lower doses than described for imaging and spectroscopic mapping in Sections 2 and 3.
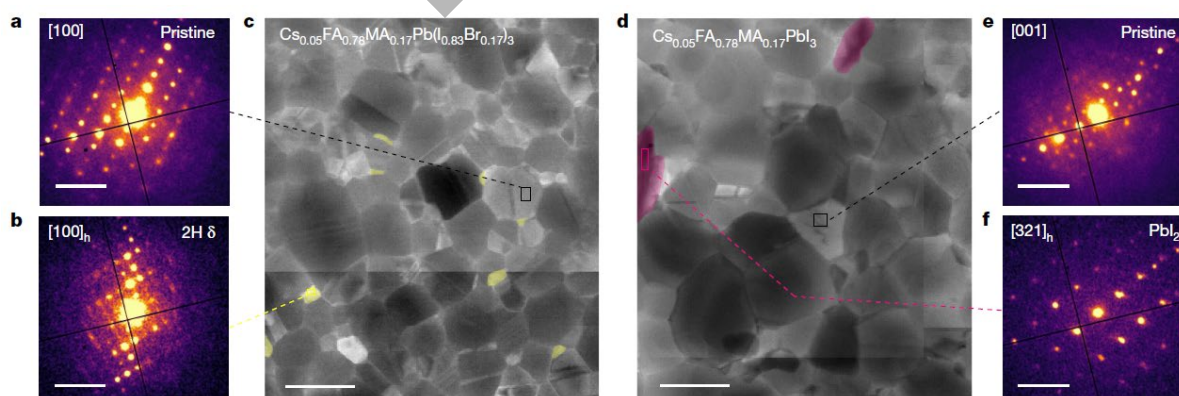

Figure 3. **a,b,** Diffraction patterns extracted from a $Cs_{0.05}FA_{0.78}MA_{0.17}Pb(I_{0.83}Br_{0.17})_3$ perovskite thin film showing a pristine perovskite grain oriented near [100] obtained from black region of interest in **c** (**a**) and a 2H δ-phase grain oriented near $[100]_h$ obtained from indicated yellow region of interest in **c** (**b**). **c,d,** Diffraction sum images extracted from SED measurements for $Cs_{0.05}FA_{0.78}MA_{0.17}Pb(I_{0.83}Br_{0.17})_3$ (**c**) and $Cs_{0.05}FA_{0.78}MA_{0.17}PbI_3$ (**d**) thin films. Yellow regions in **c** indicate hexagonal polytypes. Pink regions in **d** indicate PbI_2. **e,f,** Diffraction patterns

extracted from a $Cs_{0.05}FA_{0.78}MA_{0.17}PbI_3$ perovskite thin film showing a pristine perovskite grain oriented near [001] obtained from black region indicated in **d** (**e**) and a PbI_2 grain oriented near $[321]_h$ obtained from pink region indicated in **d** (**f**). From Reference (Macpherson *et al.*, 2022).

Summary and conclusions

Increasingly, transmission electron microscope imaging and diffraction data is being viewed as a rich data-set from which quantitative materials measurements can be made rather than the more traditional qualitative interpretation of images and diffraction patterns. There are a very wide range of established and emerging techniques to enable such metrology. Once the data is being used qualitatively, the precision of the data, or equivalent the associated error, needs to be evaluated.

Sources of error can arise from scanning distortions, noise in the experimental equipment such as read-out noise, and the quantum nature of the electrons themselves through the Poisson counting noise. Through a combination of technological improvements and post-processing methods, it is now the Poisson noise, which is the final and indeed fundamental limit to the precision. This limitation is compounded by the low electron doses that are now needed for many materials, in particular those associated with energy storage and conversion processes.

This report has highlighted work with ESTEEM3 Work Package 4 (JRA1) Imaging, Diffraction and Metrology to evaluate the precision of quantitative methods and to demonstrate their application to beam-sensitive materials. Remarkably high precisions are possible in imaging, but the comparison of the doses required between spectroscopic mapping, imaging and diffraction highlights the importance of diffraction for materials with extremely low critical doses.

References

Aarons, J., Jones, L., Varambhia, A., MacArthur, K. E., Ozkaya, D., Sarwar, M., Skylaris, C.-K. & Nellist, P. D. (2017). *Nano Letters* **17**, 4003-4012.

De Backer, A., Zhang, Z., van den Bos, K. H. W., Bladt, E., Sánchez-Iglesias, A., Liz-Marzán, L. M., Nellist, P. D., Bals, S. & Van Aert, S. (2022). *Small Methods* **6**, 2200875.

Jones, L., Varambhia, A., Nellist, P. D., Lozano-Perez, S., Griffiths, I., Beanland, R., Kepaptsoglou, D., Ramasse, Q. M., Cherns, D., Ishizuka, A., Ishizuka, K., Azough, F. & Freer, R. (2018). *Microscopy* **67**, i98-i113.

Luo, X., Varambhia, A., Song, W., Ozkaya, D., Lozano-Perez, S. & Nellist, P. D. (2022). *Ultramicroscopy* **239**, 113561.

Macpherson, S., Doherty, T. A. S., Winchester, A. J., Kosar, S., Johnstone, D. N., Chiang, Y.-H., Galkowski, K., Anaya, M., Frohna, K., Iqbal, A. N., Nagane, S., Roose, B., Andaji-Garmaroudi, Z., Orr, K. W. P., Parker, J. E., Midgley, P. A., Dani, K. M. & Stranks, S. D. (2022). *Nature* **607**, 294-300.